Experimental assessment of the sudden-reversal of the oxygen dilution effect on soot production in coflow ethylene flames

Qianlong Wang, Guillaume Legros, Jérôme Bonnety, Céline Morin, Alexis Matynia, Jean-Louis Consalvi, Fengshan Liu

Experimental assessment of the sudden-reversal of the oxygen dilution effect on soot production in coflow ethylene flames

Qianlong Wang[a,b,*], Guillaume Legros[b], Jérôme Bonnety[b], Céline Morin[c], Alexis Matynia[b], Jean-Louis Consalvi[d], Fengshan Liu[e]

[a]*Shanghai JiaoTong University, Mechanical Building A-713, School of Mechanical Engineering, Shanghai 200240, China*
[b]*Sorbonne Universités, UPMC Univ Paris 06, CNRS UMR 7190, Institut Jean le Rond d'Alembert, Paris, France.*
[c]*LAMIH CNRS UMR 8201, UVHC, F-59313 Valenciennes, France.*
[d]*Aix-Marseille Université, IUSTI/UMR CNRS 7343, 5 rue E. Fermi, 13453 Marseille Cedex 13, France.*
[e]*Measurement Science and Standards, National Research Council of Canada, 1200 Montreal Road, Ottawa, Ontario K1A 0R6, Canada.*

Abstract

This paper explores the influence of oxygen dilution on soot production when oxygen is added to the fuel stream of a steady laminar ethylene flame established over the Santoro axisymmetric coflow burner. Interestingly, at an oxygen mole fraction $\left(X_{O_2}^{ax}\right)_{trans}$ located between 30% and 32%, a transition occurs as the influence of $X_{O_2}^{ax}$ is suddenly reversed. While the peak mean soot volume fraction increases with increasing $X_{O_2}^{ax}$ within the range below $\left(X_{O_2}^{ax}\right)_{trans}$, it is reduced with increasing $X_{O_2}^{ax}$ beyond $\left(X_{O_2}^{ax}\right)_{trans}$. To help understand this transition, soot temperature and volume fraction fields are measured by the two-dimensional Modulated Absorption/Emission tech-

*Corresponding author
Email address: wangqianlong@sjtu.edu.cn (Qianlong Wang)

nique. To assess the sensitivity of the transition conditions, carbon dioxide is added to the coflowing oxidizer stream. Increasing CO_2 mole fraction in the coflow, as replacement of N_2 in the air, significantly mitigates soot formation in the flame but does not influence the transitional oxygen concentration $\left(X_{O_2}^{ax}\right)_{trans}$ within the resolution of the measurements. Due to the persistence of the transitional oxygen concentration $\left(X_{O_2}^{ax}\right)_{trans}$ over a wide range of CO_2 replacement of N_2 in the coflowing oxidizer stream, it can be considered a distinct characteristic for the assessment of numerical simulations incorporating soot formation and oxidation models. As an original database, the concomitantly measured soot temperature and volume fraction distributions are attached to the present paper as supplemental materials, thus documenting the aforementioned transitions for the whole range of CO_2 content of the coflow investigated.

Keywords: soot, soot temperature, soot volume fraction, oxygen addition, carbon dioxide dilution

---

1. Introduction

Particulate Matter (PM) and especially soot particles released to the atmosphere have been identified as a serious hazard to human health and a significant contributor to global warming [1]. Since soot exhibits a fairly short lifetime in the atmosphere on the order of days to weeks, the mitigation of soot emission has been considered as a near-term climate-change approach to gain time for implementations of long-term strategies [2]. As soot emitted by Internal Combustion (IC) engines contributes significantly to PM pollution in the air, innovative technologies especially designed for the reduction of soot emission have been a hot topic in IC engine related research in the last few decades [3–5].

The Flue Gas Recirculation (FGR) and Exhaust Gas Recirculation (EGR) are considered attractive technologies that are widely applied in industrial furnaces and IC engines to reduce the emission of pollutants. These strategies are also shown to mitigate soot release due to the reduction of both peak temperature and ignition delay for high levels of EGR dilution in Diesel engines [4]. Fundamental processes underlying FGR or EGR strategies consist of recycling part of the combustion products, either on dry or wet basis, to the fuel and/or the oxidizer of the reacting flows. Other soot emission control strategies are to dilute the fuel stream with a certain gaseous species, which is not necessarily a major component of the combustion product. As a result, the effects of such an addition on the sooting tendencies must be carefully assessed to gain a comprehensive understanding of the additive. In particular, an additive generally affects soot formation chemically and it is paramount to fully understand its chemical effects for the purpose of mitigating soot

production.

Laminar diffusion flames provide relevant conditions to investigation soot related processes, since fuel pyrolysis, soot inception, growth, and oxidation can be readily identified along the flame height. Additionally, laminar diffusion flames represent a configuration that is relevant to the assessment of sooting tendencies, as non-premixed combustion is frequently encountered in various practical combustion devices, e.g., Direct Injection (DI) engines that lead to weakly premixed combustion [6]. Therefore, studies on the sooting tendencies exhibited by laminar diffusion flames are a necessary step towards the understanding and the eventual the control of soot emissions from practical combustion devices.

As discussed by Du et al. [7] and Liu et al. [8], the reduction of soot formation resulting from the introduction of inert gaseous additives, such as N_2 or Ar, can be attributed to two main effects:

1 a dilution effect because of the reduction in the concentrations of the reactive species;

2 a thermal effect due to the change in flame temperature as a consequence of the streams' physical properties variation.

When a reactive species, such as CO_2 or O_2, is added, chemical effects also take place affecting soot formation due to the direct participation of the additive in some chemical pathways of soot formation and/or oxidation. It is worth mentioning that the flame temperature changes due to the additive chemical participation are considered as part of the chemical effects.

Though complete isolation of the chemical effect of an additive from the other two effects is impossible, several numerical and experimental studies were conducted to quantify the extent of the chemical effect [8, 9]. As an illustration, Liu et al. [8] numerically introduced a fictitious CO_2 that has exactly the same thermochemical and transport properties as real CO_2 but is not allowed to contribute to the chemical reactions. This strategy allows the CO_2 chemical effect to be isolated and assessed. The authors concluded that the chemical effects of CO_2 addition are significantly higher when CO_2 is added to the oxidizer stream where it both inhibits the formation of acetylene during the fuel pyrolysis and reduces globally the flame temperature. Gülder et al. [9] experimentally preheated the reactants to keep the theoretical adiabatic temperature constant within the whole range of O_2 and N_2 dilution levels, that is, to compensate for the thermal effect. These authors could then evaluate the magnitude of the O_2 chemical effects from the discrepancies between the levels of soot produced for O_2 and N_2 dilutions.

O_2 dilution has been largely documented in the literature dealing with laminar diffusion flames. Nevertheless, controversial results are found, since the oxygen influence seems to be altered by the fuel category and the doped side, i.e., the fuel stream or the oxidizer one. Through doping the oxidizer stream with oxygen mole fraction ranging between 9% and 50%, Glassman and Yaccarino [10] found that the sooting tendency reached a minimum in their axisymmetric ethylene flame when oxygen mole fraction is around 24%. The authors argued that increasing the oxygen mole fraction first tends to enhance soot oxidation. Concomitantly, the peak temperature is also increased, which promotes fuel pyrolysis. At some point, the latter effect pre-

vails, leading to the reversal of the oxygen dilution effect. Zelepouga et al. [11] investigated soot formation for three oxygen mole fractions (35, 50, and 100%) of the oxidizer stream in methane laminar diffusion flames, and showed that soot concentration decreased monotonically with increasing O_2 mole fraction. These authors argued that the residence time for soot particle growth is reduced as the flame length becomes smaller at higher O_2 mole fraction. Lee et al. [12] also studied the effects of O_2 addition to the coflow in laminar methane diffusion flames and found a larger soot reduction for 100% oxygen. On the contrary, in a methane counterflow configuration, increasing the oxygen content of the oxidizer stream can enhance soot formation [13].

For the purpose of studying the effect of adding oxygen to the fuel stream of a laminar coflow diffusion flame, methane, ethylene, and propane have commonly been used as the fuel and different soot formation behaviors were reported[7, 9, 14–18]. Gülder et al. [9] investigated the effects of adding oxygen and nitrogen to three fuels (methane, propane, and n-butane). These authors isolated the chemical effect from the other two (thermal and concentration dilution) experimentally. For the methane flame, oxygen addition to fuel chemically suppressed soot formation. On the opposite, oxygen addition to fuel enhanced soot formation in the propane and n-butane flames. The authors explained that the unique sooting behavior exhibited by methane is due to the reduction in acetylene concentration among the pyrolysis products as the oxygen mole fraction in the methane stream is increased. Interestingly, addition of oxygen to fuel in ethylene diffusion flames exhibits the features of these opposite trends: soot formation is first significantly promoted when increasing the oxygen mole fraction in the fuel stream, then soot formation

is abruptly reduced above a critical oxygen mole fraction of approximately 32% [7, 14, 15]. Different explanations of this sudden trend reversal were proposed. Hura and Glassman [15] suggested that the addition of a small amount of oxygen accelerates the rates of the radical formation and fuel pyrolysis. These authors speculated that the initial pyrolysis of the fuel is the crucial step in soot formation. Wright et al. [16] and Wey et al. [17] argued that the role of oxygen in promoting soot formation is due to a catalytic process rather than a thermal decomposition of the fuel as a result of the increase in temperature. Recently, in their study of soot formation in partially premixed ethylene flames, McEnally et al. [18] indicated that the increase in soot production can actually be attributed to different soot formation pathways whose magnitudes depend on the ratios of the pyrolysis products produced, but not the overall pyrolysis rate itself. The sharp decrease in soot load can then be due to the formation of double flames, i.e., an inner premixed flame and an outer diffusion flame. The changes in the hydrodynamic and thermal structures of the whole flame lead to an enhancement of soot oxidation [15]. Surprisingly, in the case of oxygen addition to a propane flame, a first decrease followed by an increase of the soot formation at oxygen mole fraction of 50% was reported by these authors [15], which was later confirmed by Liu et al [14].

Although the aforementioned studies assessed global trends of soot promotion/suppression caused by oxygen addition, the mechanisms of oxygen addition to fuel on soot formation promotion/suppression remain ambiguous. To further address the sudden-reversal behaviour in soot production of oxygen addition to fuel stream in ethylene diffusion flames, the two-dimensional

soot temperature and volume fraction fields are measured in the present paper using the Modulated Absorption/Emission (MAE) technique [19]. The laminar ethylene diffusion flames investigated in this study are established over the Santoro burner for oxygen mole fraction in the ethylene stream $X_{O_2}^{ax}$ ranging from 0 (pure ethylene) to 32% while keep the ethylene flow rate constant. As an original contribution, the sensitivity of the transitional oxygen concentration $\left(X_{O_2}^{ax}\right)_{trans}$, at which the sudden-reversal of oxygen addition to soot formation occurs, to the coflow oxidizer stream composition is assessed by replacing different amounts of nitrogen in the air with carbon dioxide. The measured soot temperature and volume fraction distributions obtained in this study are expected to constitute a valuable database for the validation of numerical models for soot formation and oxidation.

2. Experimental implementation

2.1. Burner configuration

The diffusion flames are established over an axisymmetric coflow burner identical to the one prescribed by Santoro et al. [20] and used in several previous investigations [21–24].

The central fuel stream consists of ethylene (C_2H_4) that can be oxygen diluted. Ethylene and oxygen come from high-purity gas cylinders (99.9% stated purities). Two Bronkhorst EL-FLOW mass flow controllers enable the variations of both the ethylene and oxygen flow rates, referred to as $\dot{V}_{C_2H_4}^{ax}$ and $\dot{V}_{O_2}^{ax}$, respectively. The central fuel stream flows through a vertical cylindrical brass tube with an 11 mm effective diameter of injection d_{F}. This central tube is straight over a distance of 250 mm upstream, its tip allowing the exit

velocity profile to be fully-developed over the range of investigated flow rates. In the following, $\dot{V}^{ax}$ is the overall flow rate of the central fuel stream.

The coflowing oxidizer stream consists of nitrogen, carbon dioxide, and oxygen. All these gases also come from high-purity gas cylinders (99.9% stated purities). Three other mass flow controllers allow the oxidizer stream flow rate, referred to as $\dot{V}^{co}$, together with its composition to be adjusted. In the following, $X^{co}_{O_2}$, $X^{co}_{N_2}$, and $X^{co}_{CO_2}$ are the oxygen, nitrogen, and carbon dioxide mole fractions in the coflow, respectively. The coflow oxidizer stream is delivered through the co-annular region between the central fuel tube and a concentric cylindrical brass tube of 102 mm inner diameter. A perforated brass plate, glass beads, and finally a ceramic honeycomb are used to straighten and homogenize the oxidizer flow. The central tube extends 3 mm above the honeycomb surface.

2.2. Diagnostics

The optical arrangement that enables the MAE technique has been extensively detailed in Ref.[19]. This technique provides simultaneous two-dimensional maps of soot temperature and volume fraction in the axisymmetric laminar diffusion flames investigated [24, 25].

Two continuous wave lasers operating at λ_1=645 nm (red) and λ_2=785 nm (infrared) are used as the light sources to measure the absorption fields through the flames to be investigated at both wavelengths. The selection of these wavelengths results from a trade-off between the sensitivity of the temperature measurement and the signal-to-noise ratio. Furthermore, the use of the upper part of the visible spectrum consolidates the predominance of absorption over scattering by soot particles, knowing that the participat-

ing medium is considered as non-scattering in the post-processing. As a result, the selection of λ_1 and λ_2 was proven to enable the simultaneous reconstructions of the soot temperature and volume fraction distributions with acceptable uncertainties [19].

The subsequent optical arrangement first allows both 1 mm diameter laser beams to be merged into a single one that is a combination of both wavelengths. Furthermore, the intensity of each beam can be tuned independently. The optical arrangement finally provides a collimated beam with an outgoing diameter of 70 mm. Across its section, the non-coherent light intensity is fairly uniform at both wavelengths.

After passing through the flame, the beam is decollimated with a convergent lens. Upstream the focal point a beam splitter allows the reflection of 50% intensity and the transmission of the other 50% at both wavelengths. For each laser beam, a pinhole is located at the focal point. This provides a telecentric configuration possessing depth-invariant magnification and filters the slight beam steering due to the temperature gradient that could bias the deconvolution process. Every resulting virtual image formed is re-imaged by a 12-bit progressive scan monochrome camera mounted with a conventional lens and equipped with a narrow band filter. To enable the monochromatic imaging, these filters are centered at 645 nm and 785 nm, and exhibit a band width at one half the transmissivity maximum of 20 nm and 10 nm, respectively. Every CMOS camera array is composed of 1312x1082 pixels, providing a spatial resolution of 150 μm for the projected data.

A digital pulse generator controls the occurrence and the duration of every CMOS exposure, together with the opening of the shutters that chop both

laser beams. A frame grabber records the frames captured by the cameras at a rate of 30 frames per second. In the present study, the exposure time is kept constant and set to 10ms. Although increasing the oxygen content of the central stream leads to higher peaks of flame emission rate, no saturation is found on the camera sensor over the range of investigated parameters.

2.3. Data processing

The main steps of the deconvolutions that underline the MAE technique are recalled here. The whole methodology is more specifically outlined in Ref.[19].

The flame is considered as an emitting, absorbing, and non-scattering medium. For the laminar coflow ethylene flames studied, the flame radiative spectrum in the visible is governed by the continuum radiation from soot. This is particularly true in the upper part of the visible spectrum. In addition, absorption by soot particles produced in these flames is shown to be at least one order of magnitude higher than scattering, especially at longer wavelengths in the visible [26].

In such a configuration, the Radiative Transfer Equation that models the transfer of the radiative intensity can be integrated along the optical pathways followed by both collimated laser beams inside the flame.

When the laser is off, the energy $\mathscr{E}_{\lambda}^{off}$ accumulated on a pixel during a time Δt due to the steady impinging flux emitted by the flame at wavelength

λ can then be expressed as follows:

$$\mathscr{E}_{\lambda}^{off} = \Delta\lambda\,\Delta t\,\Delta x^{pix}\,\Delta z^{pix}\,\eta_{\lambda}^{coll}\,\Omega^{coll} \int_{y_{min}}^{y_{max}} \kappa_{\lambda}(y)\,B_{\lambda}(y)\,e^{-\int_{y}^{y_{max}} \kappa_{\lambda}(y')dy'}\,dy \tag{1}$$

where $\Delta\lambda$ is the detection wavelength bandwidth, Δx^{pix} and Δz^{pix} are the impinged pixel's dimensions, Ω^{coll} is the solid angle of collection, η_{λ}^{coll} is the overall efficiency of the collection optics, y is the coordinate along the optical pathway crossing the flame between y_{min} and y_{max}, κ_{λ} is the local spectral absorption coefficient, and B_{λ} is the spectral blackbody radiative intensity at the local temperature. This intensity is given by the Planck's law:

$$B_{\lambda} = \frac{2\,h\,\pi\,c^2}{\lambda^5\left(e^{\frac{h\,c}{\lambda\,k\,T}} - 1\right)} \tag{2}$$

with k=1.3807 $\times$ 10^{-23} J/K being the Boltzmann constant, h=6.626 $\times$ 10^{-34} J·s the Planck constant, and c the speed of light in the medium, which can be considered as that in vacuum (2.998 $\times$ 10^8 m/s) in the present study.

When the laser is on, the energy $\mathscr{E}_{\lambda}^{on}$ accumulated on the same pixel is $\mathscr{E}_{\lambda}^{off}$ complemented by the energy deposited by the non-coherent collimated laser beam:

$$\mathscr{E}_{\lambda}^{on} = \mathscr{E}_{\lambda}^{off} + \Delta t\,\Delta x^{pix}\,\Delta z^{pix}\,\eta_{\lambda}^{coll}\,\phi_{\lambda}^{laser}\,e^{-\int_{y_{min}}^{y_{max}} \kappa_{\lambda}(y)dy} \tag{3}$$

In Eq.(3) ϕ_{λ}^{laser} is the incoming laser flux that can be evaluated in the absence of the participating medium, i.e. when the flame is off.

Measuring consecutively $\mathscr{E}_\lambda^{(on)}$ and $\mathscr{E}_\lambda^{(off)}$ allows the difference between both quantities to be only connected to the spectral absorption coefficient field:

$$\mathscr{E}_\lambda^{(on)} - \mathscr{E}_\lambda^{(off)} = \Delta t\, \Delta x^{pix}\, \Delta z^{pix}\, \eta_\lambda^{coll}\, \phi_\lambda^{laser}\, e^{-\int_{y_{min}}^{y_{max}} \kappa_\lambda(y) dy} \tag{4}$$

The absorption coefficient field $\kappa_\lambda(r,z)$ can then be retrieved following Eq.(4) by conducting a set of laser attenuation measurements, i.e. evaluating the left hand side (LHS) term for every pixel of the camera's sensor. The soot volume fraction field $SVF(r,z)$ can also be inferred. The Mie theory allows κ_λ to be transformed into SVF, assuming that soot particles are in the Rayleigh limit [21]:

$$SVF(r,z) = \frac{\lambda\, \kappa_\lambda(r,z)}{6\, \pi\, E(m)} \tag{5}$$

where $E(m)$ is a function of the complex refractive index m of soot.

Given the retrieved $\kappa_\lambda(r,z)$, the reconstruction of the local spectral emission rate $\kappa_\lambda B_\lambda(r,z)$ is now also allowed when measuring the LHS term in Eq.(1) for every pixel of the camera's sensor. $B_\lambda(r,z)$ can then be extracted when computing the ratio $\kappa_\lambda B_\lambda$ / κ_λ. According to Eqs.(1) and (2), the map of soot temperature $T(r,z)$ can be inferred from the field of the ratio $B_{\lambda_2}/B_{\lambda_1}$ provided the knowledge of $\eta_{\lambda_2}^{coll}/\eta_{\lambda_1}^{coll}$ together with the relationship between the intensity measured by every CMOS sensor in arbitrary unit and the absolute power impinging the sensor per unit area and per unit wavelength. To conduct the overall calibration, the beam delivered by a Halogen calibration light source is imaged on both CMOS sensors. A specific lookup

table can then be established providing T as a function of the ratio $B_{\lambda_2}/B_{\lambda_1}$ corrected for the characteristics of the CMOS sensors and the optics encompassed between the flame's location and these sensors.

In practice, each of Eqs.(4) and (1) is discretized at every height z_i imaged on a line of pixels, leading to a system of linear equations that is solved for $(\kappa_\lambda)_{ij}$ and $(\kappa_\lambda B_\lambda)_{ij}$, respectively, at the locations r_j along the line. As every set of equations is shown to be ill-conditioned, a Tikhonov regularization is used to stabilize the deconvolution process [19].

In the following, $SVF(r, z)$ is inferred from the absorption coefficient field measured at 785 nm since for a given fuel $E(m)$ tends towards a constant value when λ increases within the near infrared spectrum [27]. In addition, using the higher wavelength further consolidates the validity of the aforementioned Rayleigh limit. As proceeded in former studies [21, 28], $E(m)$ is here adjusted to 0.219 to reproduce the peak soot volume fraction measured by Santoro et al. [20] at HAB = 50 mm for ethylene burning in the air.

Furthermore, following the methodology prescribed by Legros et al. [19], confidence regions for soot temperature and volume fraction measurements can be identified according to the local relative levels of $\kappa_\lambda B_\lambda$ and κ_λ. These regions are also delineated here, guaranteeing that the measurements of soot temperature and volume fraction reported hereafter exhibit uncertainty levels lower than $\pm$50 K and $\pm$0.5 ppm, respectively. Still, the latter does not incorporate the uncertainty associated with $E(m)$ due to the ongoing debate about this quantity in the combustion community.

Finally, the fields of soot temperature and volume fraction shown in the following result from the deconvolution of the signals captured on the right

side of the flame's axis. The fields inferred from the left side of the flame lead to very similar results that do not influence the ultimate findings of the present investigations.

3. Results and discussion

3.1. Constants and parameters

The following investigations are restricted to steady flames established at the atmospheric pressure and constant room temperature of 295 K. The flow rates of ethylene and coflowing streams, i.e. $\dot{V}^{ax}_{C_2H_4}$ and $\dot{V}^{co}$, are fixed at the constant values of 0.231 l/min and 43 l/min, respectively.

As reported in Tab.1, oxygen is gradually added to the central stream at a flow rate ranging from 0 to 0.11 l/min. Consequently, the oxygen mole fraction $X^{ax}_{O_2}$ in the central fuel stream is varied between 0 and 32%, while the fuel flow rate is kept constant. This range of $X^{ax}_{O_2}$ allows the sooting tendency to be reversed as mentioned earlier for air as the coflow oxidizer [7, 14, 15]. For $X^{ax}_{O_2}$ higher than 32%, the flame burning in the air coflow starts experiencing flickering, an instability that is intimately linked to soot load at the flame tip [21, 29].

Additionally, the above parametric study is repeated for different levels of N_2 replacement by CO_2 in the oxidizer coflow summarized in Tab.2. It is noticed that the oxygen mole fraction $X^{co}_{O_2}$ of the coflow is kept constant at 21%. Thus, while the carbon dioxide mole fraction in the coflow stream $X^{co}_{CO_2}$ is increased from 0 to 37.2%, the nitrogen mole fraction $X^{co}_{N_2}$ is reduced from 79% to 41.8% correspondingly.

The range of adiabatic temperature explored for every condition of the

coflowing stream is also reported in Tab.2. Thus, the original contribution of the present study lies especially in assessing the sensitivity of the sooting tendency reversal oxygen concentration to the flame adiabatic temperature, which is significantly varied due to the wide range of CO_2 replacement of N_2 in the coflow oxidizer stream.

3.2. Flame shape

For $X^{co}_{N_2}$=79% and $X^{co}_{CO_2}$= 0, i.e., air is the oxidizer in the coflow, the evolution of the visible flame with increasing $X^{ax}_{O_2}$ is shown in Fig.1. These frames have been captured by a commercial camera with all the optical settings being identical. The equivalence ratio ϕ of the fuel stream is indicated on every frame. Within the first 8% of oxygen addition, the visible flame that initially exhibits a closed tip elongates and becomes smoking. The flame tip opens and soot escapes through the flame tip without full oxidation. This phenomenology that underlies the Smoke-Point concept [30] evidences a higher soot formation in the flame as the conditions leading to soot breakthrough at the flame tip are met.

For $X^{ax}_{O_2}$ increasing from 8% to 30%, the flame becomes brighter and the location of the peak luminosity moves upstream, i.e., approaches the tube lip, as shown in Fig.1. Meanwhile, a significant amount of soot escapes from the flame tip. Further adding oxygen up to 32%, the flame appearance is suddenly back to that for $X^{ax}_{O_2}$=8%. Beyond $X^{ax}_{O_2}$ = 32%, the flame turns to be unstable and starts showing a tendency of flashback. The above observations of the influence of oxygen addition to the ethylene flow are consistent with previous studies [14, 15]. Liu et al. [14] found that for an equivalence ratio around $\phi = 6.67$, the flashback of the ethylene flame occurred. Hura et al.

[15] reported that this flashback happened at an equivalence ratio between 6.5 and 7.3 with a similar ethylene flame and this range is hardly affected by the average flow velocity and the coflow oxygen mole fraction. In our experimental studies, the flame structure transition happens within the range $\phi = 6.8 - 6.2$ and a flame instability is triggered at a lower ϕ than 6.2.

Since the soot escapes from flame tip when $X_{O_2}^{ax}$ is at and higher than 8%, the interpretation of the visible flame height is questionable. Indeed, the flame visible emission follows a smooth decaying function in the vicinity of the flame tip. Therefore, the exact location of the final quenching of the flame and its relationship to visible emission are difficult to define and requires the definition of an arbitrary threshold. On the opposite, the mixture-strength flame height, referred to as H_f in the following, characterizes the soot inception region in the flame and can be properly identified [24]. H_f is the length measured between the burner tip (z=0 as indicated in Fig.1) and the height of the maximum local spectral soot emission rate $\kappa_{\lambda_1} B_{\lambda_1}(r, z)$. It is worth noticing that the relative trends exhibited by H_f do not depend on the selection of the wavelength. More extensive discussion about the relevance of this characteristic height can be found in Ref.[24]. As reported in Fig.1, H_f is drastically shortened as $X_{O_2}^{ax}$ is increased up to 30%. Additionally, the radial location of the maximum spectral emission rate is shown in Fig.2 as a function of the height above the burner for every $X_{O_2}^{ax}$ investigated. These profiles clearly indicate that the flame diameter is also reduced as $X_{O_2}^{ax}$ is increased up to 30%. Thus, the entire flame shrinks within this range of oxygen addition.

As the local spectral emission rate is dominated by soot radiation, the

aforementioned trends indicate that the soot inception starts earlier at a lower flame height as $X_{O_2}^{ax}$ is increased up to 30%. Meanwhile, enhanced soot inception and surface growth rates can also be anticipated, since the flame tip opens and quenching of soot oxidation occurs at a shorter length scale above the burner.

Interestingly, the evolution of the flame diameter does not match the trends reported in previous studies [20, 31]. For buoyancy-controlled coflow flame, the flame diameter is expected to be proportional to $(\dot{V}^{ax}S)^{0.25}$, where $\dot{V}^{ax}$ is the volumetric flow rate of fuel gas mixture and S the stoichiometric molar oxidizer-to-fuel ratio of the mixture [31, 32]. Still, in our measurements, the diameter decays proportionally to $\dot{V}^{ax}$ or S.

Beyond $X_{O_2}^{ax} = 30\%$, both H_f and the flame diameter start increasing again. Thus, the visible flame established for $X_{O_2}^{ax} = 32\%$ looks similar to that for 8 and 14% O_2 addition flames in Fig.1. In a more intuitive way, adding oxygen to the fuel stream now, i.e., more than 30%, enhances the overall ratio of soot oxidation to soot formation. It is reasonable to speculate that the sudden changes in the sooting tendency and the shape of the flame are attributed to an intrinsic transformation in the overall structure of reaction zone, namely the intimate coupling between the inner premixed reaction zone and the outer diffusion flame. While the potential of recovering the closed flame tip then sounds meaningful, the conditions at the flame tip for $X_{O_2}^{ax}$ higher than 32% lead to flickering. As unsteady effects on soot production require special attention [33], these are beyond the scope of the present paper.

3.3. Soot volume fraction and temperature fields

Fields of soot volume fraction (left) and temperature (right) are shown in Fig.3 for $X_{N_2}^{co}$=79%, $X_{CO_2}^{co}$= 0, and different $X_{O_2}^{ax}$. Due to the limited collimated laser beam, the flame cannot be probed beyond z = 70mm.

As $X_{O_2}^{ax}$ is increased from 0 to 30%, the net peak SVF in the flame increases 45.3 ppm. Furthermore, at lower $X_{O_2}^{ax}$ (0 - 20%), the location of the peak SVF remains in the annular region of the flame. In contrast, when the oxygen fraction rises up to 30%, the peak SVF is shifted downstream. Thus, the soot layer structure inside the flame has changed. Beyond the flame transition, i.e. for $X_{O_2}^{ax}$ = 32%, the topology of the measured soot volume fraction and temperature fields turn to be similar to the initially non-premixed flame, although the flame can be considered as a more premixed-like flame, i.e. an inner premixed flame and an outer diffusion one, which is in agreement with the observations by Hura and Glassman [15]. Liu et al.[14] also suggested that the suppression of soot formation by a large amount of oxygen addition is due to the premixed nature of the fuel stream.

According to the calculated theoretical adiabatic flame temperature, the temperature grows by approximately 230K for $X_{O_2}^{ax}$ increasing from 0 to 32% (see Tab.2). However, the topology of the temperature field measured in the flame does not follow a uniform increase. For $X_{O_2}^{ax}$ up to 30%, the soot temperature tends to be reduced in the upper region of the flame, while it increases within the lower outer annular region of the flame, where the higher soot spectral emission rate lies. As stated in the former section, a higher soot inception rate is anticipated with higher $X_{O_2}^{ax}$, which is probably caused by changes of the chemical pathways producing the pyrolysis products [18].

Consequently, the global enhancement of soot formation by oxygen addition to ethylene could be explained in this following way: within the inner soot inception region, oxygen-induced PAHs formation pathway is highly promoted; meanwhile, in the subsequent soot growth and oxidation regions, the oxidation rate is slowed down due to the soot temperature decrease, which results in higher level of soot escaping from the flame without full oxidation. Thus, the higher soot loading in the upper regions of the flame is largely a direct consequence of the higher soot formation rates in the lower regions. This is in agreement with the observations reported by Axelbaum and Law [34]. To the authors' knowledge, this is supported here for the first time by simultaneous measurements of soot temperature and volume fraction distributions. These experimental data are useful for model validation and are therefore provided as supplemental materials.

3.4. Assessment of the oxygen chemical effect

To assess the effects of oxygen addition to fuel on soot loading, the mean soot volume fraction $F_{soot}(z)$ is defined as follows

$$F_{soot}(z) = \frac{4}{\pi\, d_F^2} \int_0^{d_F/2} 2\,\pi\, r\, SVF(r,z)\, dr \tag{6}$$

$F_{soot}(z)$ represents the visible flame cross-section mean soot volume fraction at a given HAB in the flame.

Figure 4 displays the evolution of $F_{soot}(z)$ for different $X_{O_2}^{ax}$ with air being the oxidizer in the coflow ($X_{O_2}^{co}$=21%, $X_{N_2}^{co}$=79%, $X_{CO_2}^{co}$=0%). As $X_{O_2}^{ax}$ is increased from 0 to 30%, the slope of the increasing part of $F_{soot}(z)$ raises monotonically. Concomitantly, the peak F_{soot}, referred to as F_{max} from now

on, increases while it is shifted upstream. For $X_{O_2}^{ax} = 32\%$, the profile of $F_{soot}(z)$ experienced a dramatic trend reversal. Its increasing part is very similar to that measured for $X_{O_2}^{ax} = 8\%$ while F_{max} is located at a HAB similar to that shown for $X_{O_2}^{ax} = 14$ %. This again is a clear indication that the overall flame structure has undergone a sudden change.

Furthermore, Wang et al. stated that F_{max} characterizes the soot formation rate in the flame [24]. As a result, it can also be selected as an indicator to discriminate the relative contributions of the dilution and chemical effects caused by oxygen addition. Thus, the evolution of F_{max} with varying additive content of the fuel stream is shown in Fig.5. The magnitude of the evolution is scaled by the value of F_{max} for pure ethylene ($X_{O_2}^{ax} = 0$) burning in the air, i.e., $F_{max} = 2.1$ ppm. Here, the baseline is provided by the results obtained for N_2 dilution of the fuel stream and extracted from Ref.[24]. As oxygen and nitrogen exhibit similar heat capacities and molecular diffusivities, the thermal effect caused by N_2 and O_2 is largely canceled out in this relative scale. Therefore, the relative chemical effect of oxygen addition can be quantitatively assessed when subtracting the N_2 dilution effect. The magnitudes of both effects are illustrated by the black arrows in Fig.5.

Thus, the chemical effect of oxygen addition to the fuel stream drastically promotes soot formation and dominates the dilution effect. For $X_{O_2}^{ax} = 30\%$, the chemical effect is approximately 10 times higher than the dilution effect. Beyond this level, the chemical effect remains significant but soot formation then drops sharply.

3.5. Combined effects of the coflow composition and oxygen addition on the sooting tendency

As stated before, the sudden trend reversal in sooting tendency that occurs beyond $X_{O_2}^{ax} = 30\%$ is a unique transition for oxygen addition to the ethylene stream. One can then wonder how persistent this transitional oxygen concentration is when the coflowing oxidizer compositions are modified. Carbon dioxide addition to the coflowing stream has been shown to significantly influence the sooting tendency of the ethylene diffusion flame established over a very similar burner configuration. Additionally, the influence of such an addition can be considered a relevant investigation for refined understanding of the actual EGR effect on sooting tendencies, as mentioned in the Introduction. Consequently, the above parametric study is repeated for a set of different carbon dioxide contents $X_{CO_2}^{co}$ of the coflow, which were achieved by replacing different levels of N_2 with CO_2 while keeping the mole fraction of O_2 constant at 21%. Thus, the flames established with the conditions of the fuel stream specified in Tab.1 experience gradual substitutions of nitrogen in the coflow oxidizer stream by carbon dioxide following the conditions summarized in Tab.2. Doing so, the hydrodynamic conditions at the burner inlets are kept constant. It is worth noticing that the momentum conditions are then modified, as the density of carbon dioxide is higher than that of nitrogen. However, for such buoyancy driven laminar flames, the effect of this modification is believed to be negligible. Within the range of $X_{O_2}^{co}$ investigated, i.e. 0 - 37.2%, the theoretical adiabatic temperature is then significantly spanned over a range whose magnitude is approximately 570 K (see last column in Tab.2).

As a result, a total of 30 different flames are investigated. Following the data post-processing outlined above, the associated SVF and soot temperature fields are also processed and provided in the supplemental material.

A selection of the aforementioned fields are shown in Fig.6 for a set of $X^{co}_{CO_2}$, i.e. 10.5%, 18.6%, and 32.5%. To highlight the potential similarities and/or discrepancies among the expected transitions of the sooting tendencies, every field of SVF is shown in a non-dimensional way, with the reference value being the peak SVF (SVF_{max}) measured among the set of $X^{ax}_{O_2}$ investigated for a given $X^{co}_{CO_2}$. These reference values are reported on the left of every row. As reported in past studies investigating both short chain fuels [8, 9] and longer ones [22, 35], carbon dioxide significantly mitigates soot formation when it is added to the coflowing oxidizer stream. As a result, $\mathrm{SVF}_{\mathrm{max}}$ is monotonically reduced from 57.4 ppm met for $X^{co}_{CO_2}$=10.5% and $X^{ax}_{O_2}$=30% down to 39.4 ppm for $X^{co}_{CO_2}$=32.5% and $X^{ax}_{O_2}$=30%. Meanwhile, at any $X^{ax}_{O_2}$, the soot temperature is globally reduced as $X^{co}_{CO_2}$ is increased. These observations are especially in agreement with the findings by Liu et al. [8] who attributed these trends to the CO_2 chemical effect that mitigates acetylene formation along with the fuel pyrolysis.

Despite this significant alteration of $\mathrm{SVF}_{\mathrm{max}}$, it is remarkable to notice that the sudden-reversal of the flame sooting tendency happens within the same range of $X^{ax}_{O_2}$, i.e., between 30% and 32%, for all $X^{co}_{CO_2}$ investigated. In addition, the overall variation of the sooting trends with increasing oxygen addition to fuel is very similar to that depicted for $X^{co}_{CO_2}$=0 (see Fig.3). With increasing $X^{ax}_{O_2}$ up to 30%, the soot formation rate is enhanced and the peak soot volume fraction is shifted inwards and downstream. Meanwhile, the

peak soot temperature is shifted upstream in the annular region of the flame while the inner downstream soot temperature decreases. For $X_{O_2}^{ax} = 32\%$, the sudden-reversal in sooting tendency happens at all levels of CO2 replacement and the peak soot volume fraction shifts upstream and appears in the wing of the flame.

The profiles of F_{soot} shown in Fig.7 are restricted to the range of $X_{O_2}^{ax}$ encompassing the conditions of the transition. For every $X_{CO_2}^{co}$ investigated, F_{max} is actually obtained for $X_{O_2}^{ax}$ between 30% and 32%. Thus, the addition of carbon dioxide to the coflow does not enable any significant modification of the oxygen content in the fuel stream required for the sudden-reversal in the flame sooting tendency.

Finally, all F_{max} evaluated contribute to an experimental database that can yield a map of F_{max} as a function of $X_{O_2}^{ax}$ and $X_{CO_2}^{co}$ (see Fig.8). To this end, a local two-dimensional interpolation has been conducted based on either a cubic spline for the inner conditions ($X_{O_2}^{ax}$, $X_{CO_2}^{co}$) or a bilinear regression for the conditions located at a boundary of the investigated domain. For legibility, the color scale is intentionally coarse to enable the identification of the contours. The vertical blue dotted line indicates once more clearly the very weak influence of $X_{CO_2}^{co}$ on the transition of the sooting tendency. Intuitively, the absolute soot loading is indeed reduced as more CO_2 is added to the coflow stream. In contrast, carefully inspecting the domain of conditions below $X_{O_2}^{ax}$=30%, the distance along the $X_{O_2}^{ax}$ axis between two neighboring isolevels of F_{max} becomes closer within increasing $X_{CO_2}^{co}$. This indicates that the carbon dioxide addition to the coflow further enhances the potential of oxygen addition to the ethylene stream to hasten soot formation. An alter-

native way to illustrate this non-intuitive trend is to plot the variation of the normalized maximum F_{soot} with $X_{O_2}^{ax}$ for different levels of CO_2 replacement of the coflow stream, i.e., different $X_{CO_2}^{co}$, as shown in Fig.5. Fig.5 evidences that at a given level of oxygen addition to fuel, $X_{O_2}^{ax}$, the relative enhancement in soot loading induced by the chemical effect of oxygen addition increases with increasing levels of CO_2 replacement of the coflow stream.

These counter intuitive results may be explained by the different effects of CO_2 and O_2 added to the coflow oxidizer and fuel streams, respectively, on soot formation. In the case of pure ethylene in the fuel stream, i.e., without oxygen addition, and air as the oxidizer in the coflow, the temperatures in the centerline region just above the burner exit are relatively low and soot nucleation in the centerline region occurs at a distance relatively downstream. It is well-known that adding CO_2 to the coflow stream lowers both soot nucleation and soot surface growth rates, not only through its thermal and dilution effects, but also through its chemical effect. Although the majority of soot mass is attributed to soot surface growth, soot nucleation also plays a crucial role in the overall soot process. As such, addition of CO_2 to the coflow stream is effective to lower the peak soot volume fraction. On the other hand, when a certain amount of oxygen (less than 30%) is added to the fuel stream, the oxygen-induced fuel pyrolysis leads to rapid temperature rise in the centerline region above the burner exit and produces abundant radicals and soot precursor species, leading to earlier soot nucleation with higher rates. It is therefore reasonable to assume that the CO_2 added to the coflow stream plays a less role in soot nucleation suppression than that when there is no oxygen added to the fuel stream, though CO_2 may still

play a similar role in suppressing the soot surface growth process. As a result, oxygen addition to fuel prompts soot formation more significantly in the relative sense, compared to the case without oxygen addition to the fuel stream, as more CO_2 is added to the coflow oxidizer stream through replacement of nitrogen.

3.6. Discussion

Although the probed section of the flame is limited by the 70 mm diameter laser beam, the SVF fields measured allow for F_{max} to be clearly identified for every condition investigated (see Figs.4 and 7).

Moreover, it is worth noticing that for $X_{O_2}^{ax}$=0, $X_{CO_2}^{co}$=37.2%, and $X_{O_2}^{co}$=21%, the flame flickers, therefore is not documented in the measurement. As a result, no field is provided for these conditions in the supplemental material. Katta et al. [29] shown that a flickering methane jet diffusion flame can be stabilized when enhancing the soot formation through acetylene addition to the methane stream. These authors indicated that the higher soot radiation results in a temperature drop which in turn suppresses the buoyancy-induced instability. In our study, moving $X_{O_2}^{ax}$ from 0 to 8% results in a higher soot volume and a lower temperature at the flame tip while the flame becomes stable. The flame stabilization mechanism behind these two cases deserves more attention but further investigations are out of this paper's scope.

In addition, for $X_{O_2}^{ax}$=0, $X_{O_2}^{co}$=21%, and $X_{CO_2}^{co}$ beyond 32.5%, though the SVF fields can still be decently retrieved, the soot temperature field could not be due to the very low level of emission signals, which leads to unacceptably large uncertainties in the measurements. For this reason, the soot

temperature fields are not available under these conditions in the supplemental material.

4. Conclusion

In this work, the variations of flame geometry, soot volume fraction, and soot temperature in axisymmetric laminar ethylene flames are systematically investigated as O_2 is added to the fuel stream of the Santoro burner stabilized ethylene diffusion flames. The shrinkage of both mixture-strength flame height and flame diameter are reported with increasing $X_{O_2}^{ax}$ from 0 to 30%. Confirming previous investigations, a flame transition occurs for $X_{O_2}^{ax}$ between 30% and 32%. This transition is associated with a sudden drastic reduction in soot formation, which is an indication of some intrinsic transformation in the overall flame structure. Employing the Modulated Absorption/Emission technique, the present study provides detailed distributions of soot temperature and volume fraction before and at this transition. The promoted soot formation is probably caused by a shift in the pathways of fuel pyrolysis, which results in higher concentrations of soot precursor species, leading to higher soot nucleation and surface growth rates. The large amount of soot at the flame tip is likely a consequence of the higher soot formation rates in the soot inception and growth regions and the lower soot oxidation rates due to decreased temperatures associated with excessive radiation heat loss by soot.

Moreover, within the range of $X_{O_2}^{ax}$ investigated, the chemical effect induced by oxygen dominates the dilution effect and promotes soot formation in the flame. For $X_{O_2}^{ax} = 30\%$, the chemical effect is approximately an order

of magnitude higher than the dilution effect.

Finally, the impact of the coflow compositions on the influence of the oxygen addition on soot formation has been explored for the first time. It was found that increasing the CO_2 mole fraction in the coflow oxidizer stream while keeping the oxygen mole fraction at 21% contributes to the mitigation of soot formation in the flame, but has essentially no influence on the transitional oxygen concentration $\left(X_{O_2}^{ax}\right)_{trans}$ in the fuel stream that results in the sudden-reversal in the flame sooting tendency. The measured distributions of soot temperature and volume fraction at different levels of oxygen addition to the fuel stream along with the remarkably stable transitional oxygen mole fraction of about 31% in ethylene constitute a valuable database for validation of flame models incorporating sophisticated mechanisms of soot formation/oxidation.

Further optical developments will allow the MAE technique to be complemented by a measurement of the mean soot particle diameter. Indeed, the present setup will be added a third laser beam operating at a wavelength that is sensitive to light diffusion, i.e. to particle size [36]. Thus, the database will be complemented by the fields of mean soot particle diameter, a crucial information that will especially remove the uncertainty associated with the speculated trends on soot growth rates.

Acknowledgments

The authors feel grateful to the Chinese Scholarship of Council together with the France Centre National d'Etudes Spatiales for their grants. The present study has been supported by the China Postdoctoral Science Foun-

dation (NO. 2016M591672)

[1] R.A. Kerr, Soot is warming the world even more than thought, *Science* 339 (2013) 382.

[2] H.A. Michelsen, C. Schulz, G.J. Smallwood, S. Will, Laser-induced incandescence: particulate diagnostics for combustion, atmospheric, and industrial applications, *Prog. in Energy Combust. Sci.* 51 (2015) 2–48.

[3] Z. Gao, W. Schreiber, The effects of EGR and split fuel injection on diesel engine emission, *Inter. Journ. Automotive Tech.* 2 (2001) 123 –133.

[4] M. Yao, Q. Zhang, H. Liu, Z. Zheng, Diesel engine combustion control: medium or heavy EGR? *SAE Technical Paper* 2010-01-1125 (2010).

[5] J. Jang, Y. Lee, C. Cho, Y. Woo, C. Bae, Improvement of DME HCCI engine combustion by direct injection and EGR, *Fuel* 113 (2013) 617-624.

[6] A. Maiboom, X. Tauzia, J.F. Hétet, Experimental study of various effects of exhaust gas recirculation (EGR) on combustion and emissions of an automotive direct injection diesel engine, *Energy* 33 (2008) 22-34.

[7] D.X. Du, R.L. Axelbaum, K.C. Law, The influence of carbon dioxide and oxygen as addtives on soot formation in diffusion flames, 23^{rd} *Sympo. (Inter.) on Combust.* 23 (1990) 1501–1507.

[8] F.S. Liu, H.S. Guo, G.J. Smallwood, The Chemical Effects of Carbon Dioxide as an Additive in an Ethylene Diffusion Flame: Implications for Soot and NO_x Formation, *Combust. Flame* 125 (2001) 778–787.

[9] Ö. Gülder, Effects of Oxygen on Soot Formation in Methane , Propane , and n-Butane Diffusion Flames, *Combust. Flame* 101 (1995) 302–310.

[10] I. Glassman, P. Yaccarino, The Effect of Oxygen Concentration on Sooting Diffusion Flames, *Combust. Sci. Technol.* 24 (1980) 10–114.

[11] S. A. Zelepouga, A.V. Saveliev, L. A. Kennedy, A. A. Fridman, Relative effect of acetylene and PAHs addition on soot formation in laminar diffusion flames of methane with oxygen and oxygen-enriched air, *Combust. Flame* 122 (2000) 76–89.

[12] K. Lee, A. V. Saveliev, L. A. Kennedy, Soot Formation Effects of Oxygen Concentration in the Oxidizer Stream of Laminar Coannular Nonpremixed Methane/Air Flames, *Combust. Flame*121(2000) 323–333.

[13] A. Beltrame, P. Porshnev, W. Merchan-Merchan, A. Saveliev, A. Fridman, L.A. Kennedy, Soot and NO formation in methane-oxygen enriched diffusion flames, *Combust. Flame* 124 (2001) 29–310.

[14] F. Liu, K. Thomson, J. Gregory, Experimental investigation of oxygen addition to fuel on soot formation in laminar coflow diffusion flames of ethylene and propane, *Proc. of the IMECE2006*, 2006.

[15] H.S. Hura, I. Glassman, Soot formation in diffusion flames of fuel/oxygen mixtures, 22^{nd} *Sympo. (Inter.) on Combust.* 22 (1988) 371–378.

[16] F.J. Wright, Effect of oxygen on the carbon-forming tendencies of diffusion flames, *Fuel* 53 (1974) 232–235.

[17] C. Wey, E.A. Powell, J.I. Jagoda, The effect on soot formation of oxygen in the fuel of a diffusion flame, 20^{th} *Sympo. (Inter.) on Combust.* 20 (1984) 1017–1024.

[18] C. S. McEnally, L.D. Pfefferle, B. Atakan, K. Kohse- H öinghaus, Studies of aromatic hydrocarbon formation mechanisms in flames: Progress towards closing the fuel gap, *Progress in Energy Combust. Sci.* 32 (2006) 247–294.

[19] G. Legros, Q. Wang, J. Bonnety, M. Kashif , C. Morin, J.-L. Consalvi, F. Liu, Simultaneous soot temperature and volume fraction measurements in axis-symmetric flames by a two-dimensional modulated absorption/ emission technique, *Combust. Flame* 162 (2015) 2705–2719.

[20] R.J. Santoro, H.G. Semerjian, R.A. Dobbins, Soot particle measurements in diffusion flames, *Combust. Flame* 51 (1983) 202–218.

[21] M. Kashif, J. Bonnety, P. Guibert, C. Morin, G. Legros, Soot volume fraction fields in unsteady axis-symmetric flames by continuous laser extinction technique, *Opt. Exp.* 20 (2012) 28742–28751.

[22] M. Kashif, J. Bonnety, A. Matynia, P. Da Costa, G. Legros, Sooting propensities of some gasoline surrogate fuels: Combined effects of fuel blending and air vitiation, *Combust. Flame* 161 (2015) 1840–1847.

[23] G. Legros, T. Gomez, M. Fessard, T. Gouache, T. Ader, P. Guibert, P. Sagaut, J.L. Torero, Magnetically induced flame flickering, *Proc. Combust. Inst.* 33 (2011) 1095–1103.

[24] Q. Wang, G. Legros, J. Bonnety, C. Morin, Experimental characterization of the different nitrogen dilution effects on soot formation in ethylene diffusion flames, *Proc. Combust. Inst.* 36 (2017) 3227–3235.

[25] A. Jocher, H. Pitsch, T. Gomez, G. Legros, Dual magnetic effects on soot production in partially premixed flames, *Proc. Combust. Inst.* 36 (2017) 1377–1385.

[26] F. Liu, D.R. Snelling, K.A. Thomson, G.J. Smallwood, Sensitivity and relative error analyses of soot temperature and volume fraction determined by two-color LII, *Appl. Phys. B* 96 (2009) 623-636.

[27] J. Yon, R. Lemaire, E. Therssen, P. Desgroux, A. Coppalle, K.F. Ren, Examination of wavelength dependent soot optical properties of diesel and diesel/rapeseed methyl ester mixture by extinction spectra analysis and LII measurements, *Appl. Phys. B* 104 (2011) 253-271.

[28] A. Jocher, H. Pitsch, T. Gomez, G. Legros, Modification of sooting tendency by magnetic effects, *Proc. Combust. Inst.* 35 (2015) 889–895.

[29] V.R. Katta, W.M. Roquemore, A. Menon, Impact of soot on flame flicker, *Proc. Combust. Inst.* 32 (2009) 1343-1350.

[30] G.H. Markstein, J. De Ris, Radiant emission and absorption by laminar ethylene and propylene diffusion flames *Proc. Combust. Inst.* 20 (1985) 1637-1646.

[31] J.H. Kent, H.Gg. Wagner, Why do Diffusion flames Emit smoke *Combust. Sci. Tech.* 41(1984) 245- 269.

[32] J.H. Kent, H.Gg. Wagner, Temperature ang fuel effects in sooting diffusion flame, 20^{th} *Sympo. (Inter.) on Combust.* 20 (1984) 1007-1015.

[33] P. Rodrigues, B. Franzelli, R. Vicquelin, O. Gicquel, N. Darabiha, Unsteady dynamics of PAH and soot particles in laminar counterflow diffusion flames *Proc. Combust. Inst.* 36 (2017) 927–934.

[34] R.L. Axelbaum, C.K. Law, Soot formation and inert addition in diffusion flames, 23^{rd} *Sympo. (Inter.) on Combust.* 23 (1990) 1517–1523.

[35] M. Kashif, P. Guibert, J. Bonnety, G. Legros, Sooting tendencies of primary reference fuels in atmospheric laminar diffusion flames burning into vitiated air, *Combust. Flame* 161 (2014) 1575–1586.

[36] H. Zhao, B. Williams, R. Stone, Measurement of the spatially distributed temperature and soot loadings in a laminar diffusion flame using a Cone-Beam Tomography technique, *J. Quant. Spectrosc. Radiat. Transf.* 133 (2014) 136–152.

List of Figures

$\dot{V}^{ax}_{C_2H_4}$ (l/min)	$\dot{V}^{ax}_{O_2}$ (l/min)	$X^{ax}_{O_2}$
	0	0
	0.02	8%
	0.04	14%
0.231	0.06	20%
	0.09	28%
	0.10	30%
	0.11	32%

Table 1: Experimental parameters of the central stream.

$\dot{V}^{co}$ (l/min)	$\dot{V}^{co}_{O_2}$ (l/min)	$X^{co}_{O_2}$	$\dot{V}^{co}_{N_2}$ (l/min)	$X^{co}_{N_2}$	$\dot{V}^{co}_{CO_2}$ (l/min)	$X^{co}_{CO_2}$	adiabatic temperature (K)
43	9	21 %	34	79 %	0	0	[2567 - 2800]
			29.5	68.5%	4.5	10.5%	[2459 - 2687]
			26	60.4%	8	18.6%	[2383 - 2607]
			22	51.1%	12	27.9%	[2302 - 2522]
			20	46.5%	14	32.5%	[2265 - 2483]
			18	41.8%	16	37.2%	[2229 - 2444]

Table 2: Experimental parameters of the coflowing stream. For every line, the range of adiabatic temperature is evaluated over the range of conditions for the central stream specified in Tab.1

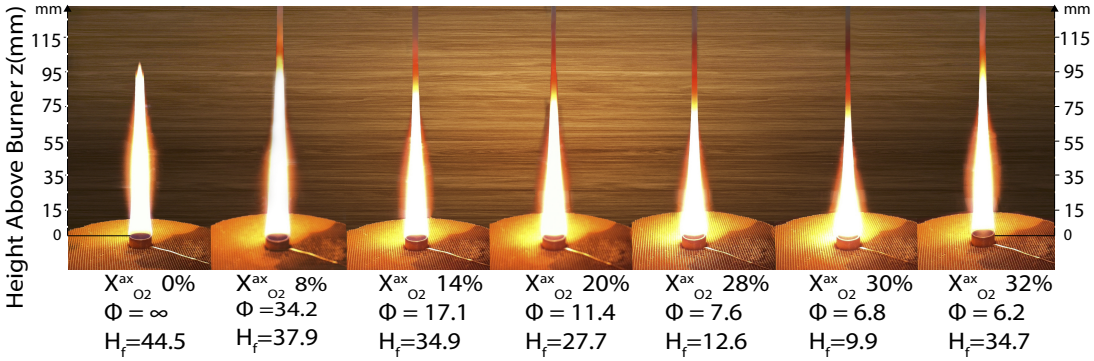

Figure 1: Evolution of the visible flame with increasing $X_{O_2}^{ax}$ for air ($X_{O_2}^{co}$=21%, $X_{N_2}^{co}$=79%, $X_{CO_2}^{co}$=0%) in the coflow. Flow rates are given in Tabs.1 and 2.

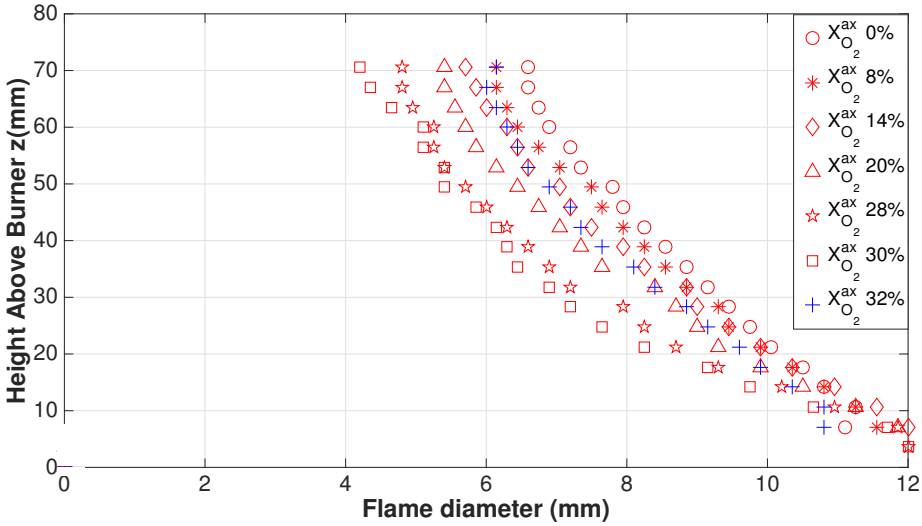

Figure 2: Evolution of the flame diameter with increasing $X_{O_2}^{ax}$ for air ($X_{O_2}^{co}$=21%, $X_{N_2}^{co}$=79%, $X_{CO_2}^{co}$=0%) in the coflow. Flow rates are given in Tabs.1 and 2.

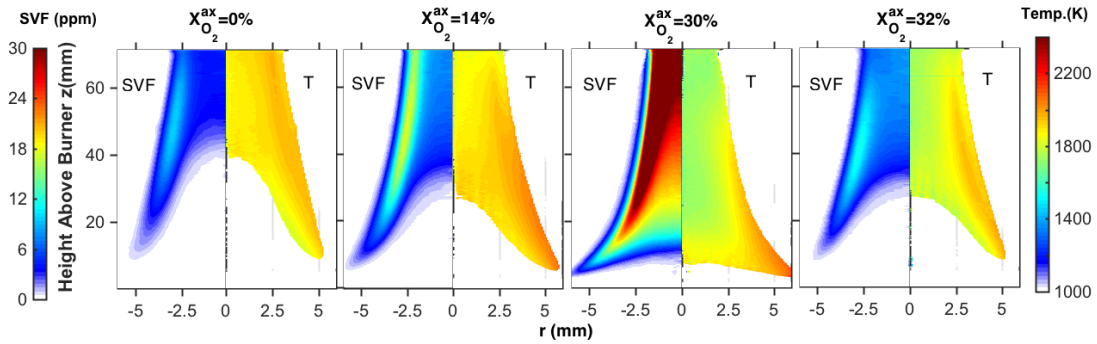

Figure 3: Evolution of the two-dimensional soot volume fraction (left side) and temperature (right side) fields with increasing $X_{O_2}^{ax}$ for air ($X_{O_2}^{co}$=21%, $X_{N_2}^{co}$=79%, $X_{CO_2}^{co}$=0%) in the coflow. Flow rates are specified in Tabs.1 and 2.

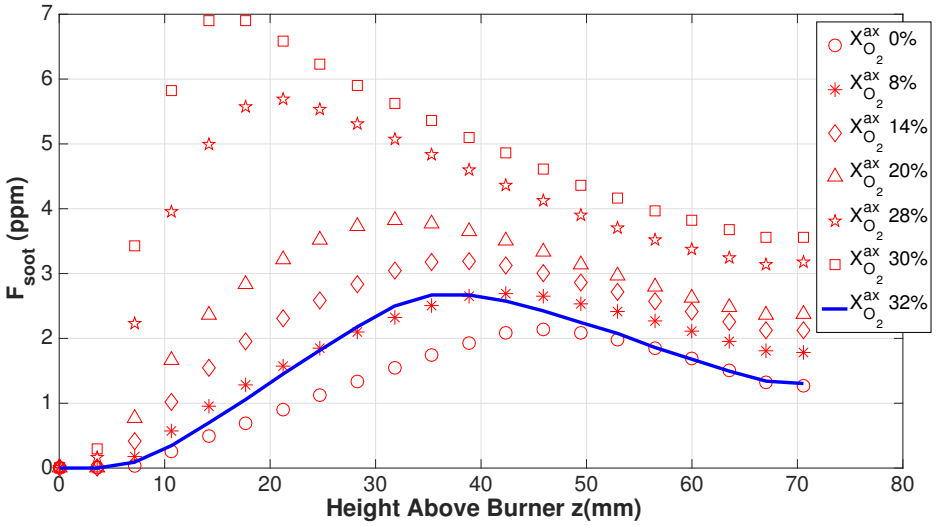

Figure 4: Evolution of the mean soot volume fraction F_{soot} for air ($X^{co}_{O_2}$=21%, $X^{co}_{N_2}$=79%, $X^{co}_{CO_2}$=0%) in the coflow and different $X^{ax}_{O_2}$. Flow rates are specified in Tabs.1 and 2.

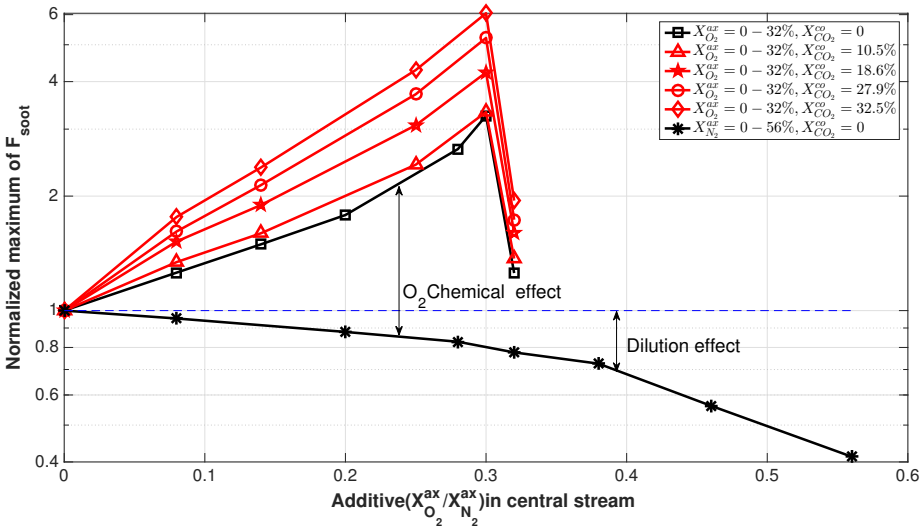

Figure 5: Variation of the relative dilution and chemical effects of $X^{ax}_{N_2}$ and $X^{ax}_{O_2}$ on the flame sooting tendency for different $X^{co}_{CO_2}$. The data are normalized with respect to the reference undiluted condition. N_2 dilution results are from Ref.[24].

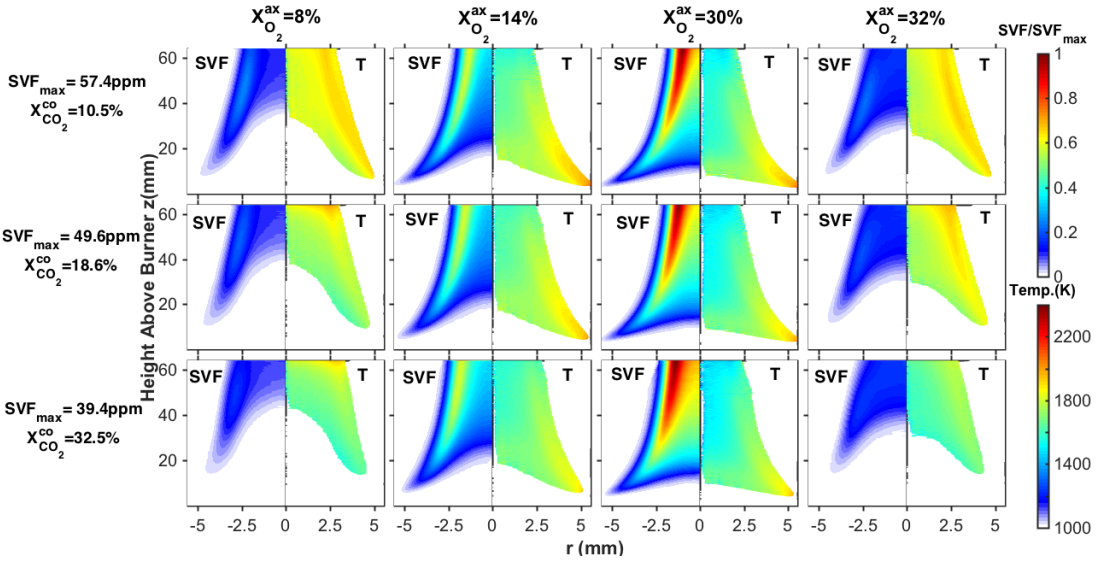

Figure 6: Two-dimensional soot volume fraction (left side) and temperature (right side) fields for increasing $X^{ax}_{O_2}$ (from the left to the right) and increasing $X^{co}_{CO_2}$ (from the top to the bottom). For every $X^{ax}_{O_2}$, the soot volume fraction measurements are normalized by the maximum measured among the conditions explored along the corresponding row. Experimental conditions are given in Tabs.1 and 2.

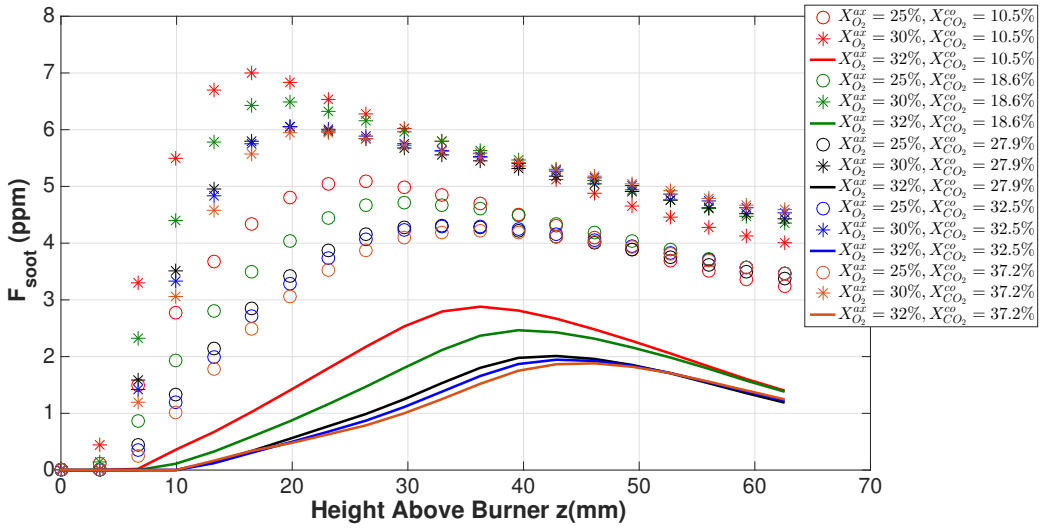

Figure 7: Evolution of the mean soot volume fraction F_{soot} for different $X_{O_2}^{ax}$ and $X_{CO_2}^{co}$. Flow rates are specified in Tabs.1 and 2.

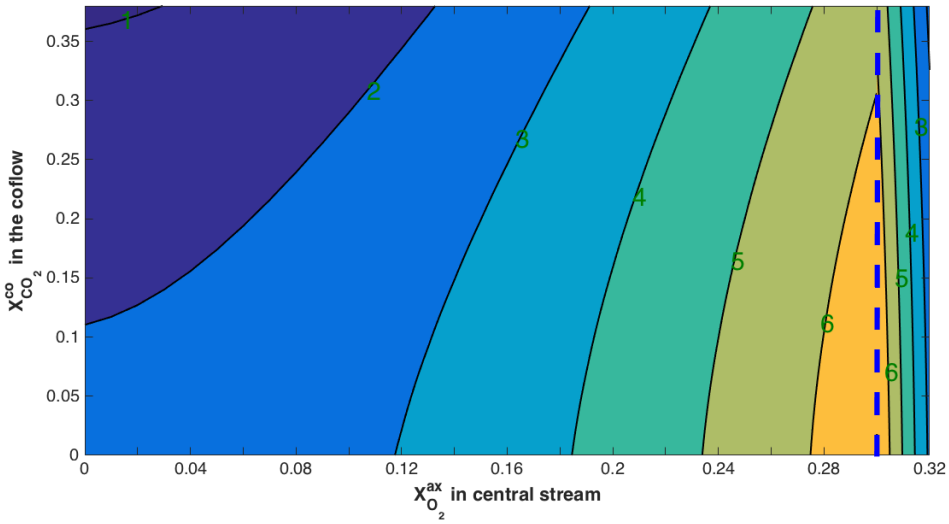

Figure 8: Variation of F_{max} (ppm) with $X^{ax}_{O_2}$ and $X^{co}_{CO_2}$.